Optics and Lasers in Engineering 152 (2022) 106945

Contents lists available at ScienceDirect

Optics and Lasers in Engineering

journal homepage: www.elsevier.com/locate/optlaseng

Single-camera stereoscopic 3D multiplexed structured image capture for quantitative fuel-to-air ratio mapping

Walker McCord, Cary Smith, Zhili Zhang*

Department of Mechanical, Aerospace, and Biomedical Engineering, University of Tennessee, Knoxville, TN 37996, USA

ARTICLE INFO

Keywords:
Three-dimensional
Multiplexed structured image capture
Chemiluminescence
Fuel-to-air ratio
Flame

ABSTRACT

A single-camera three-dimensional Multiplexed Structured Image Capture (3D-MUSIC) based stereoscopic imaging system is demonstrated to obtain a three-dimensional fuel-to-air ratio (FAR) map of a methane-air Bunsen flame at standard atmosphere conditions. Images of the C_2^* (500nm) and CH^* (430nm) emissions are spatially modulated and captured through two optical paths and combined into a single image on the camera. The C_2^* / CH^* ratio is computationally recovered by low-pass filtering in the spatial frequency domain and exhibits a linear trend to a FAR map of the flame. Each channel's unique FAR map is fused to generate a line-of-sight three-dimensional FAR map by triangulating points from each channel's perspective. As an imaging technique, the 3D MUSIC is capable of obtaining multi-spectral multi-view 3D images using spatial modulation and recovery in one camera without any special illumination. It may be extended for applications in combustion, biomedical, and other key diagnostics.

1. Introduction

Non-intrusive optical diagnostic techniques have become indispensable tools for researchers to study the complex and hostile environment often associated with combustion processes and propulsion applications. Scientifically, many open questions still exist in the understanding of the governing processes of turbulent flames and chemistry, therein better knowledge of these processes will pave ways for increased combustion efficiency, emission monitoring, and reduced environmental impacts. Established experimental techniques, such as Coherent Anti-Stokes Raman Scattering (CARS) [1], spontaneous Raman scattering [2], flame chemiluminescence emission [3], and planar laser-induced fluorescence (PLIF) [1] have provided great insight about turbulence, combustion chemistry, and their interactions. However, many of these techniques have been limited to single-point, line, or planar measurements [4,5]. Turbulent flames by nature are inherently three dimensional (3D), thus to best understand flame characteristics including flame topology, evolution, gradients, and dissipation rates time-resolved three-dimensional measurement techniques are needed [6]. Advancements in high-speed imaging and advanced reconstruction algorithms have made it feasible for 3D measurement techniques of turbulent flames to achieve the needed level of spatiotemporal resolutions to provide unprecedented insight into their dynamic behavior [7,8]. There are several approaches that currently or have been explored and the techniques fall under two general categories, computed tomography (CT) or a sweeping planar technique [8]. Generally, a CT technique has a more simplified setup and alignment, but has difficulty seeing into the body of the flame and requires multiple high-speed intensified cameras with advanced synchronization and control electronics. A sweeping planar technique has added cost and complexity of multiple lasers, but can see into the body of the flame for a more comprehensive measurement [9].

In this work, a passive 3D imaging technique based on structured detection is proposed and demonstrated: two-channel Multiplexed Structured Image Capture (3D - MUSIC), which can be used for multi-spectral, multi-view 3D imaging applications. 3D MUSIC is used to reconstruct a target object and a 3D FAR map of a methane/air Bunsen flame. The MUSIC technique has been described in previous work [10–13]. MUSIC uses the spatial modulation of light prior to imaging to encode a target scene into spatial frequency shifts, with each shift corresponding to a unique spectral or temporal image and resulting in individual distinct snapshots. The scene could be multi-spectral, time-evolving, or independent, and the encoding allows the elements of interest to be individually tagged as sub-images. Therefore, a single-shot multiplexed exposure of the scene will be composed of the overlapped tagged sub-images. Taking the Fourier transform of the image resolves the spatial frequency shifts associated with the tagged elements, as shown by Eq. (1):

$$\tilde{I}_G(\vec{k},t)=\sum_{n=1}^{N}[\varepsilon_n I_n(\vec{k},t)\otimes\sum_{m=-\infty}^{\infty}\frac{2\sin(mk_0T_1)}{m}\delta(k_{xn}-mk_0)] \tag{1}$$

* Corresponding author.
E-mail address: zzhang24@utk.edu (Z. Zhang).

https://doi.org/10.1016/j.optlaseng.2021.106945
Received 7 June 2021; Received in revised form 7 December 2021; Accepted 30 December 2021
Available online 11 January 2022
0143-8166/© 2022 Elsevier Ltd. All rights reserved.

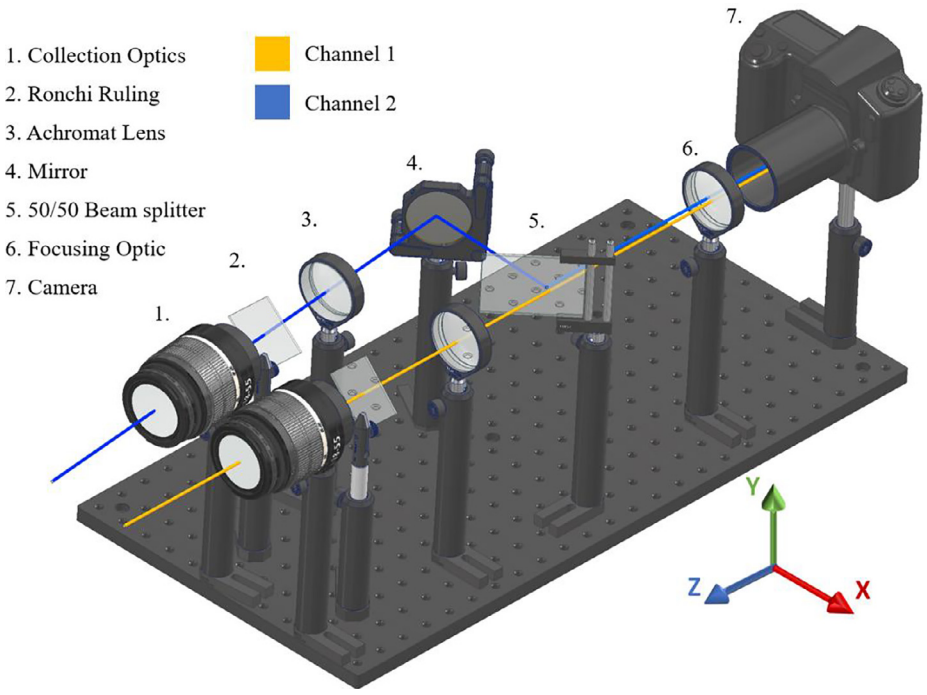

Fig. 1. Diagram of the experimental setup for 3D MUSIC. The angle between channel 1 and 2 is 6 degree to minimize the mean error reprojections during calibration. The x-y-z coordinate system is shown.

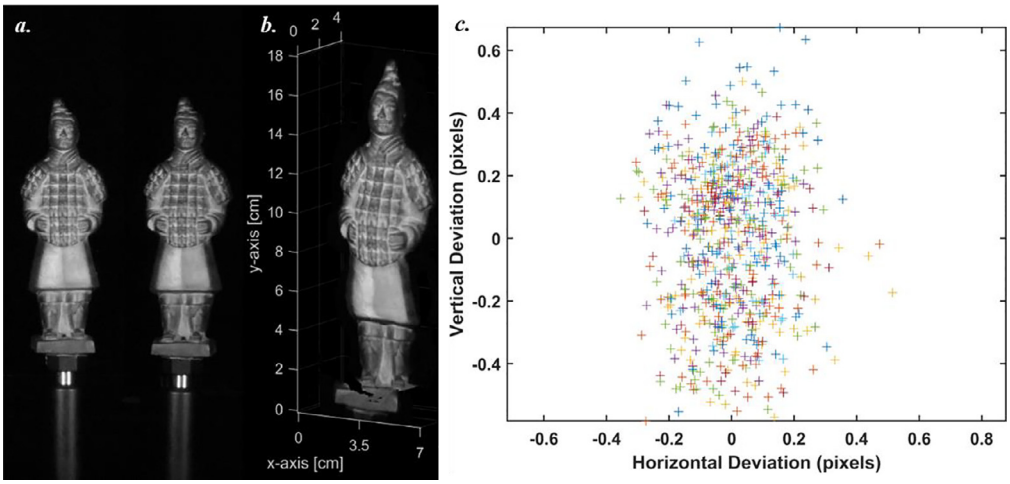

Fig. 2. (a) Channel one & two views of a statue (b) 3D reconstruction based on the two views from (a), (c) Calibration fidelity, showing reprojection errors obtained from checkerboard target

In this equation, the tagged information for N sub-images contained in the original image $\tilde{I}_G$ is resolved in the Fourier domain as a function of each tagged element I_n with optical efficiency ϵ_n, convolved with the Fourier transform of the modulation pattern represented periodically by T_1 wherein k_0 and k_{xn} are the modulation pattern's fundamental frequency and path-specific spatial frequency variable respectively. Post-processing of the multiplexed snapshot using a recovery algorithm for isolating the frequency shifts via low-pass filtering extracts the unique tagged elements from the frequency domain and thus enables individual reconstruction of the scene's sub-images [12]. Finally, the fusion of multiple views into a 3D map is conducted. It should be noted that the temporal resolution of MUSIC can be controlled by various imaging arms, up to sub nanosecond [10].

Traditional systems that implement a stereo-adaptor to achieve unique views by splitting the CCD chip have been around for many years. The adaptor allows for a robust and compact optical design with minimal alignment needed for stereo-imaging. By analyzing the unique views and identifying small discrepancies in feature details; algorithms can output a depth map of the imaged scene. This process, known as stereovision, has been used extensively in entertainment, medical, and automated systems [14]. Furthermore, the technique has been expanded by adding multiple prisms to provide up to 4-views per sensor, but there are inherent drawbacks to using these adapters. First, due to the splitting of the CCD chip, these systems can only be applied to small objects with limited size, whose projection size must be smaller than half the sensor array; else detrimental overlap may occur. Second, adaptor systems that incorporate a bi-prism result in distortions induced by the nonlinear angle variation and different lateral displacement, which become more severe depending on wedge angle [15,16]. An advantage to implementing structured detection into a stereovision system is that, unlike stereo adapters, MUSIC allows the full sensor size to be used for each view albeit a slight degradation in resolution from the recovery process. The reduced spatial resolution is not as critical as sensor area preservation; as an earlier study on capabilities and limitation of stereovision found there was a linear degradation in 3D recovery resolution as average signal intensity per view decreases [16]. Commonly, setups utilize high-speed intensified cameras to achieve CT with adequate signal; however, such cameras are often limited to 1024 × 1024 sensor or

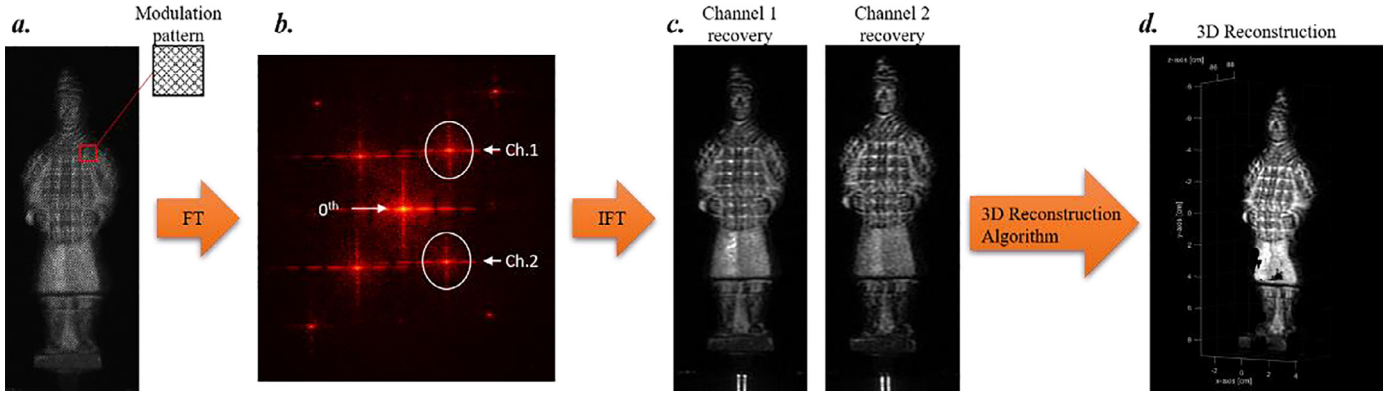

Fig. 3. Flow diagram detailing the process of 3D MUSIC. (a) the single-shot multiplexed image of the statue using the experimental setup in Fig. 1, the insert is zoomed in to show the spatial modulations of the image, (b) Spatial Fourier transformation of the (a), showing separate peaks at different spatial frequencies, (c) Inverse Fourier transformation of low-pass filtered (b) to recover the individual scenes from channel 1 and 2. (d) 3D reconstruction of the (c) to generate 3D view of the statue.

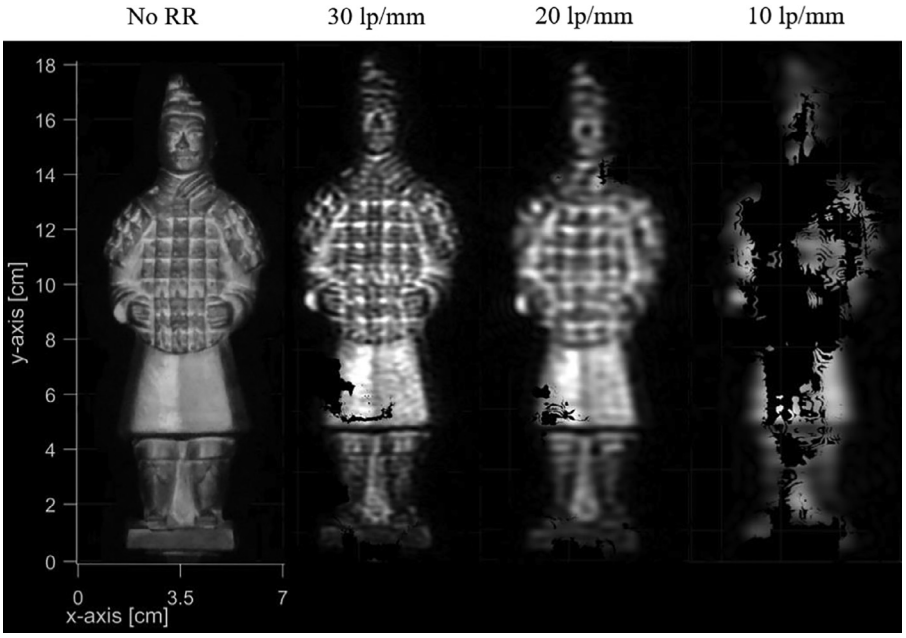

Fig. 4. Illustrated how various gratings affect density and detail of the 3D reconstruction. No RR means no Ronchi ruling and the images are taken separately for reconstruction. 10 lp/mm, 20lp/mm, 30 lp/mm mean that the images are multiplexed by gratings with 10 lines per mm, 20 lines per mm and 30 lines per mm, respectively.

less, expanding upon the importance of MUSIC's sensor area preservation capability.

2. Experimental setup

A representation of the experimental setup is shown in Fig. 1. First, the target scenes are collected by the two camera lenses with different angular displacement and projected through channels 1 and 2, respectively. Ronchi rulings with different offset angles are placed at the first focal planes to spatially modulate the incoming scenes, from which achromatic lenses are used to relay the images further into the system. A 50/50 beam splitter recombines the two channels and a focusing lens is used to image the multiplexed scenes onto a camera sensor. It should be noted that the diagram resembles a typical consumer DSLR camera, which can be replaced with any imaging device pertinent to a particular experiment. The unique modulation patterns of the Ronchi rulings allow for individual scene reconstruction from the multiplexed image through post processing. To achieve stereo vision, the channel two optics are placed 12.5 cm in the x-direction and rotated 6 degrees in the y-axis with respect to channel one. The y-axis rotation is chosen such that a central point is reciprocated in both channels' views and allows for two distinct views. The collection optics used are Nikon AF-P DX 18-55mm camera lenses with f/3.5 and are focused onto a plane tangent to the nearest point of the Bunsen flame. All objects are placed 84 cm away from the face of channel 1 camera lens in the z-direction. The entire setup is housed on an optical breadboard.

For FAR measurements, a half-inch diameter (1.27 cm) Bunsen burner with methane/air flame was used. The Bunsen burner has been a main component in scientific labs for decades and provides a stable bright flame, which is ideal for the FAR measurements conducted in this study. The Bunsen flame has a fuel-rich premixed inner flame and a diffusion outer flame: CO and H_2 from the inner flame encounter ambient air, which leads to different local FAR than the global FAR. Fuel and air flow rates were controlled using electronic flow meters (OMEGA) that allowed for easy adjustment of the global equivalence ratios during testing. A metal collar was machined for the burner that sealed the threaded expansion joint and allowed for controlled air flow input. The total flow rate of fuel and air was held at 11 SLPM. Due to the high overall flow rate and small flame nozzle, it was found the flame would auto-extinguish for equivalence ratios below 0.95, thus the ratios used ranged from 1.00 to 1.40 in increments of 0.05. An ICCD Scientific grade camera (PI-MAX4, Princeton Instruments) with a 1024 × 1024 pixel ar-

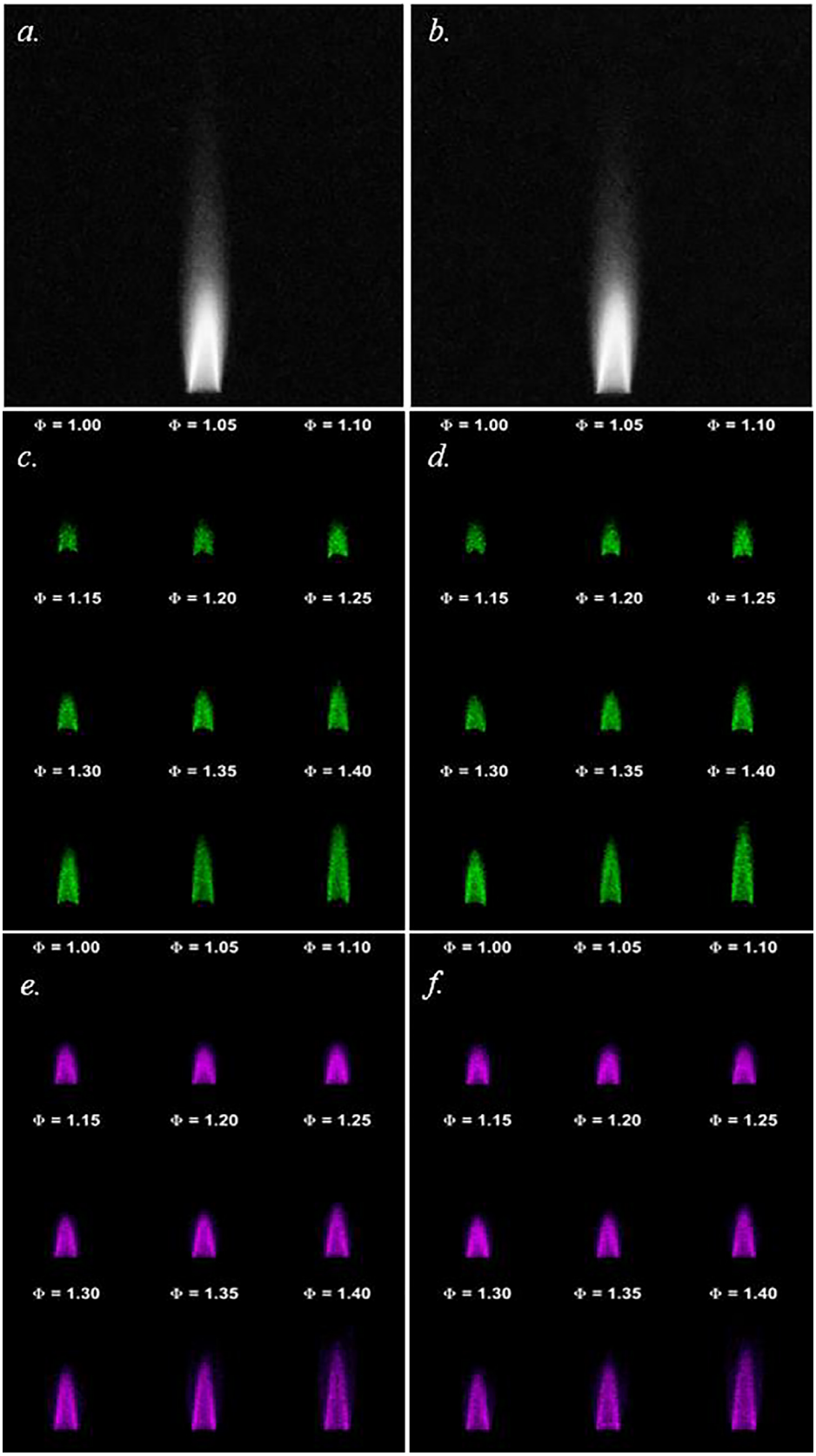

Fig. 5. (a and b) Ground truth images: Unfiltered Bunsen flame image as seen by Channel 1 and Channel 2, respectively. (c & d) Recovered images of C2 emissions at 514.5 nm (FWHM 10±2 nm) from multiplexed Bunsen flame images at various global equivalence ratios for Channel 1 and Channel 2, respectively. (e & f) Recovered images of CH emissions at 433 nm (FWHM 10±2 nm) from multiplexed Bunsen flame images at various equivalence ratios for Channel 1 and Channel 2, respectively.

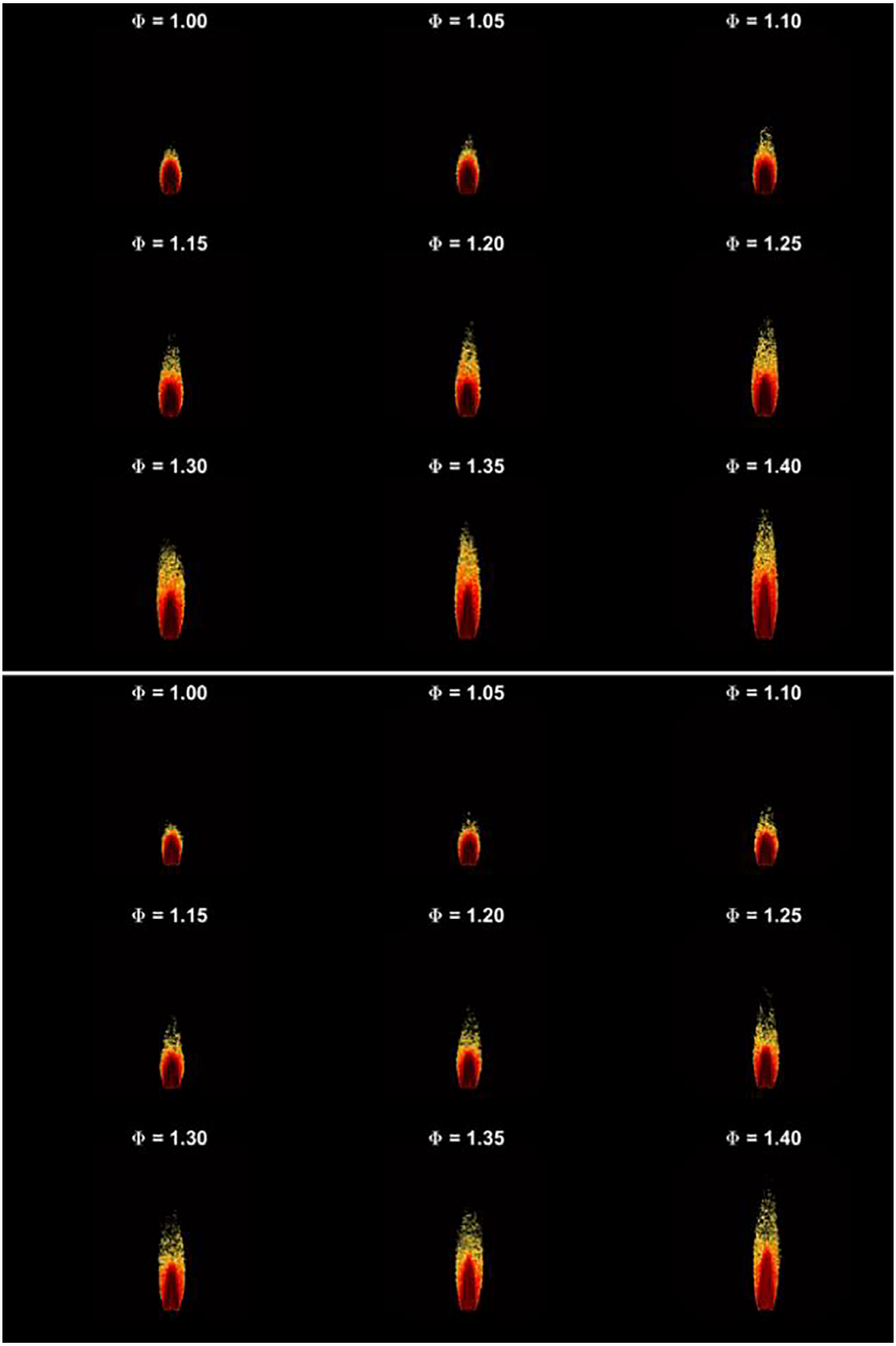

Fig. 6. 2D ratio images of recovered C_2^*/ recovered CH^* for channel 1 (top) and channel 2 (bottom), indicting good fidelities for the recovered images from the multiplexed flame images.

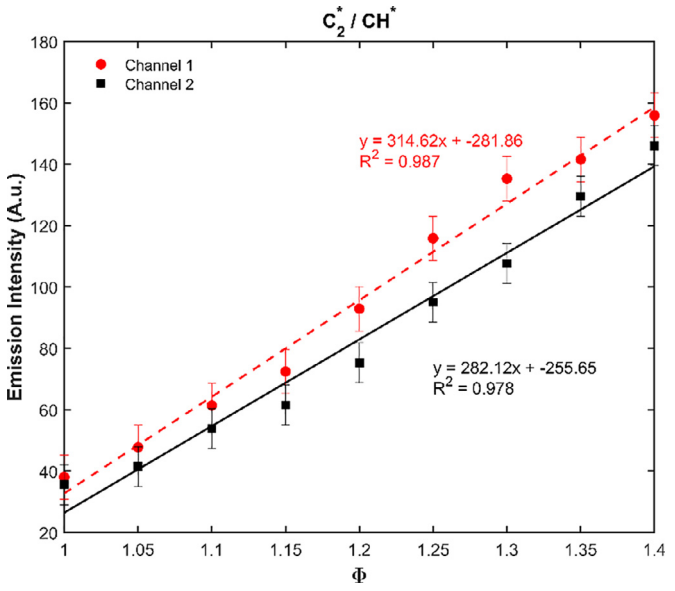

Fig. 7. Global equivalence ratio dependence on the ratio of recovered C2*/ recovered CH* for channel 1 and channel 2, indicting good fidelity of the MUSIC reconstruction for the multiplexed images.

ray was used to record the flame chemiluminescence emission. A camera gate width of 300μs and gain of 40 resulted in the best signal-to-noise ratio (SNR) for chemiluminescence images. For equivalence ratio imaging and mapping, bandpass spectral filters at 433 nm (FWHM 10±2 nm) and 514.5 nm (FWHM 10±2 nm) were used for CH* and C_2* respectively.

3. Results and discussion

3.1. Fidelity of 3D reconstruction

From a computational point of view, if a 3D scene is represented by two unique views, the recapture of the information depth is possible when the scene information is combined with knowledge of sensor geometry. Thus, channels one and two were treated as if they were distinct views. A checkerboard calibration target with squares measuring 23 × 23mm was imaged multiple times at varying angles, heights, and distances from the collection optics. These images were multiplexed onto the camera sensor, and then using the MUSIC technique, recovered. The recovered images were processed via a calibration algorithm that has been well documented in past literature [17,18]. The camera calibration process results in the systems extrinsic and intrinsic properties as well as, the reprojection errors. Extrinsic properties refer to the camera placement in the world coordinate system and intrinsic properties relate to the lens, tangential, and skew distortions. Furthermore, reprojection error is the mean distance error in pixels between the detected and re-projected points. The system used achieved a mean reprojection error of 0.25 pixels and a depth of field of ±50mm. Mathematically, given the smallest allowed disparity increments Δd, the smallest achievable depth range resolution from the camera ΔZ can be determined by Eq. (2).

$$\Delta Z = \frac{Z^2}{fT}\Delta d \tag{2}$$

Where, f is the focal length and T is the distance between the two channels collection optics. Image rectification was performed, reducing the 2D correspondence problem to a 1D problem, greatly reducing the computational time needed. Shown in Fig. 2. are ground truth images of a statue, 3D reconstruction, and corresponding reconstruction fidelity.

The number of variables and factors that go into the stereo calibration and reconstruction technique is beyond the scope of this paper. 3D MUSIC makes use of an established and well documented technique that has been extensively covered in past literature [17–22]. The use of the stereo reconstruction technique with minor modifications yielded dense and accurate three-dimensional point maps of an object. Fig. 3 gives a diagrammatic overview of how a multiplexed image becomes a 3D reconstruction.

One of the constraints for 3D reconstruction fullness and quality is the upper limit of post-recoverable information from the MUSIC technique. MUSIC is prone to resolution loss due to the low-pass filtering in the spatial frequency domain. Generally, the low-pass filters have upper spatial frequency limits determined by the need to isolate the region of interest from interference by other harmonics. The allowable filter size is thus governed by the max distance between harmonics in the spatial frequency domain, this spacing is determined by the density of the Ronchi grating, i.e. a finer grating increases the distance between features and vice versa in the spatial frequency domain [10].

To examine the impacts of the grating fineness on the overall 3D reconstruction, 10, 20, and 30 lines per mm (lp/mm) gratings were selected, and the recovered images were used to reconstruct the object in a 3D world plane. Fig. 4 shows the comparison of 3D reconstruction using various gratings. When the images are taken separately without multiplexing by Ronchi ruling, the reconstruction can show almost all the details of the sculpture, which can be regarded as the ground truth. When the two images are simultaneously imaged via multiplexing, the minor loss of some fine details are obvious. As the object is multiplexed at lower spatial resolutions, greater information loss is incurred until reconstruction failure occurs. The large discrepancy in both reconstruction quality and population density between 30 and 10 lp/mm is a result of separation distance of strong features in peaks in the Fourier domain and dictates allowable filter size. It was found the filtered area for the 30 lp/mm Ronchi ruling was greater by a factor of 10.24 when compared to the filter size area for the 10 lp/mm. Thus, the 30 lp/mm grating was solely used for encoding the rest of the data presented. It should be noted the intensities for the reconstructed images have greater contrast than the original reconstruction due to the filtering technique and the way the images color pallet was visualized.

3.2. 3D chemiluminescence FAR map using single-camera 3D MUSIC

Fig. 5 shows the chemiluminescence imaging results for the Bunsen flame using 2-channel 3D MUSIC system. Fig. 5(a) and (b) show the unfiltered images of the flame. The images were obtained by blocking one of the channels without multiplexing, so that the images can be regarded as the ground truth images. As the equivalence ratio increases, there is a strong visual increase of emitted C_2*. CH* is a radical that is highly dependent on temperature and is prominent in fuel rich conditions, thus CH* emission is strongly seen in the inner core and faintly seen in the outer regions of the flame body. At atmospheric pressure, the ratio of C_2*/CH* exhibits a linear trend that can be used to determine a flame's FAR map [3].

Fig. 5 (c)–(f) are reconstructed images from a single multiplexed image for each equivalence ratio. The C_2* spectra imaged at the various equivalence ratios for channel 1 and channel 2 are shown in Fig. 5(c), (d). The CH* spectra imaged at the various equivalence ratios for channel 1 and channel 2 are shown in Fig. 5(e), (f). Two identical bandpass filters were placed in each channel for imaging the spectra. The multiplexed image was then processed and the unique scenes were recovered. Furthermore, the resolution loss due to the filtering in the recovery method is minimal with negligible induced artifacts.

There are several key steps to reconstruct 3D FAR map from multiplexed images. Although the FAR map is found by taking the ratio of the C_2* over CH* from the reconstructed images, the 3D FAR map requires reconstructed images at the highest quality to ensure global FAR accuracy. First, images for C2* and CH* of the same channel were ratioed to

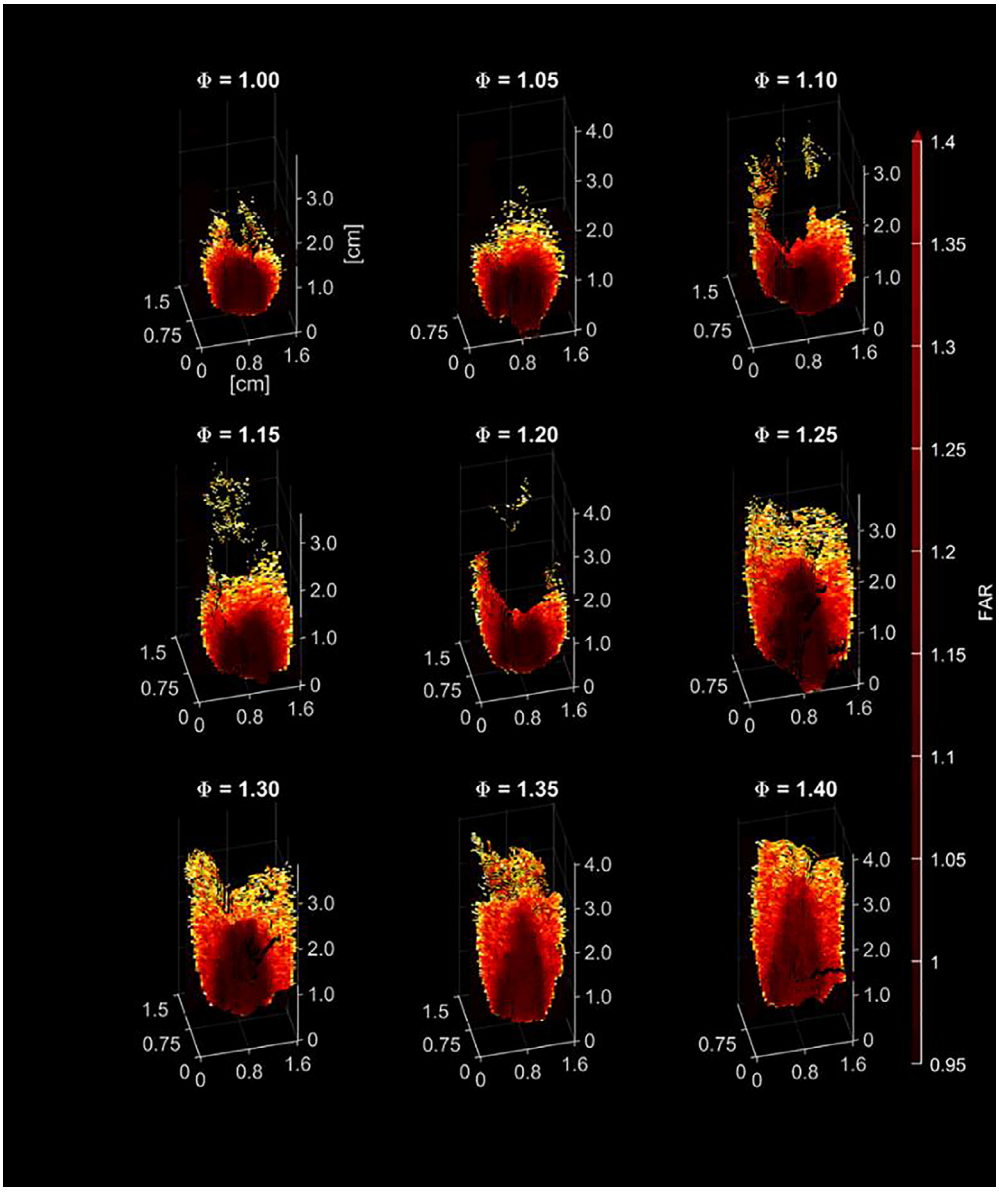

Fig. 8. 3D local FAR reconstructions of Bunsen flame at different equivalence ratios.

obtain a 2D map. Second, the linear trend line of the ratio emission intensity from channel 1 and channel 2 is found, which allows for the 3D FAR mapping by equating the images to the relations. Last, using the reconstruction algorithm, features and similar ratio values were matched to produce a 3D reconstructed FAR map.

Fig. 6 shows the 2D ratio images of recovered C_2^* over recovered CH^* for channel 1 and channel 2, respectively, which are the basis images for 3D reconstruction. The images were obtained by taking the ratios of the recovered C_2^* and CH^* images from channel 1 and channel 2 in Fig. 5. Additionally, 100-shot averaged background was removed from each image prior to processing. The images in Fig. 6. were averaged and taking care to only include flame emission signal and excluding background noise. This resulted in an average emission intensity of the C_2^*/CH^* signal at the varying equivalence ratios for each respective channel. The averaged values of C_2^*/CH^* versus global equivalence ratios were plotted and a linear trend line was fitted, as shown in Fig. 7. Curve fitting the data resulted in R^2 values of 0.987 and 0.978 for channel 1 and channel 2, respectively; this is in excellent agreement with prior literature of non-multiplexed measurements [3]. Channel 1 exhibits a slightly higher slope and an overall greater intensity when compared to channel 2, as a direct result of additional reflections from added optical elements.

Fig. 8 shows 3D reconstructions of the FAR maps for the flames at the varying equivalence ratios. This map shows the FAR values of the flame at any world coordinates in x, y, and z-location. The reconstruction algorithm was able to place the flame in real-world space to within a tolerance of ±0.05 mm. The 3D ratio image for equivalence ratio of 1.35 is shown in Fig. 9. at various viewpoints to better illustrate the system's ability to reconstruct the flame. It should be noted that reconstructions for global equivalence ratios of 1.10 and 1.20 had the highest discrepancy error leading to areas of the flame with relatively low intensity in the upper-center part of the flame.

The 3D FAR maps shown in Figs. 8 and 9 were found to accurately show the C_2^*/CH^* ratio in a calibrated 3D volume. Note that at the outer regions of the flame the FAR map begins to exceed the upper limits of the predicted equivalence ratio. This is expected, as CH^* is highly temperature dependent and as the flame temperature falls off near the outer regions spectral emission significantly decreases. This phenomenon has been documented in past literature that examined the CH^* emission of a flame body in 3D space [23–25]. As a direct result of this, the 3D

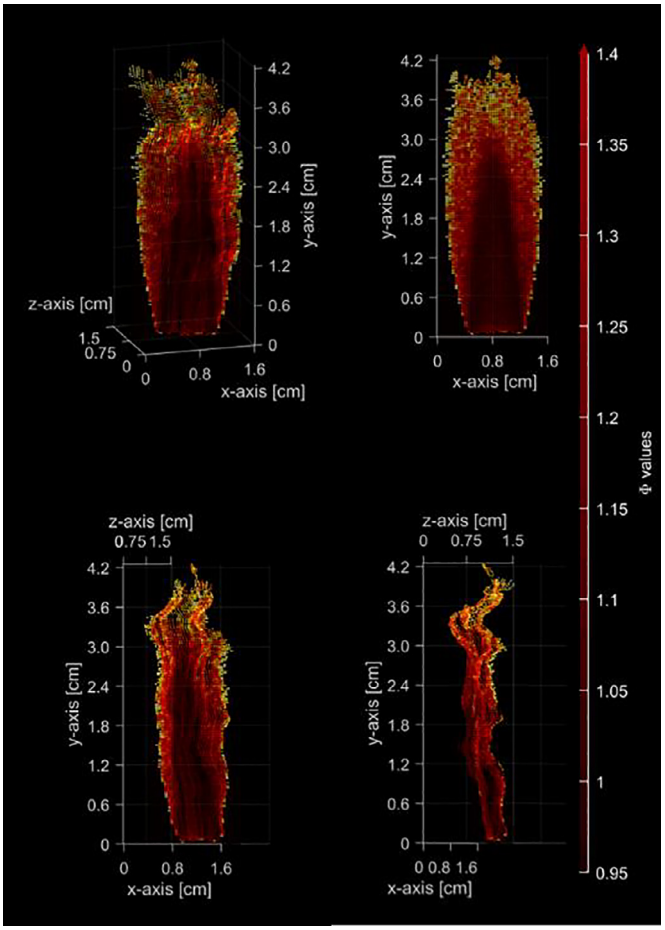

Fig. 9. Various viewpoints of the 3D FAR map of the Bunsen flame at global equivalence ratio of 1.35.

FAR map sees a rapid jump in ratio values near the outer regions of the flame body. Furthermore, 3D-MUSIC application is not limited to single-shot imaging. A series of images were captured with the flame rotated 90° between snapshots. These images were reconstructed and stitched together to represent an encompassing 3D FAR map (see Visualization 1).

4. Conclusions

This work has demonstrated the stereoscopic imaging ability of the Multiplexed Structured image Capture (MUSIC) technique using a single camera. The system was optimized by examining various focal lengths, modulation gratings, and object depth that yielded dense 3D reconstructions. MUSIC post-processing code was used to recover the multiplexed images. The recovered images were processed through an established 3D reconstruction algorithm that matched values and features to visualize a 3D FAR map of methane/air flames at varying equivalence ratios. The system was able to reconstruct the 3D FAR map with measurable placement errors of ±0.05 mm.

The 3D-MUSIC technique is capable of 3D imaging by increasing the number of views per camera while still maintaining full sensor size per view, which can be used for many challenging diagnostic techniques in combustion, biomedicine, and additive manufacturing. This negates the downfalls associated with sensor splitting, which is more apparent in the use of intensified scientific cameras with limited sensor sizes. Furthermore, 3D-MUSIC 2nd channel translational distance is only limited by the time-of-flight constraint for a given capture speed. Theoretically the 2nd channel could be moved further away from the system and act as a new view. Furthermore, 3D MUSIC would be capable of expanding beyond two channels to possibly three or more. 3D MUSIC's capability of utilizing one camera per two full scenes would allow for the effective number of cameras utilized in stereo imaging applications to be cut in half, drastically reducing the experimental cost associated with multiple high-speed intensified cameras.

Declaration of Competing Interest

The authors declare that they have no known competing financial interests or personal relationships that could have appeared to influence the work reported in this paper.

CRediT authorship contribution statement

Walker McCord: Investigation, Data curation, Writing – original draft. **Cary Smith:** Investigation, Data curation, Writing – original draft. **Zhili Zhang:** Conceptualization, Supervision, Project administration.

Funding

This work is supported by University of Tennessee, NSF-2026242 and DOE.

Supplementary materials

Supplementary material associated with this article can be found, in the online version, at doi:10.1016/j.optlaseng.2021.106945.

References

[1] Eckbreth AC. Laser diagnostics for combustion temperature and species, 3. CRC press; 1996.
[2] Jiang N, et al. High-speed 2D Raman imaging at elevated pressures. Opt Lett 2017;42(18):3678–81.
[3] McCord W, et al. Quantitative fuel-to-air ratio determination for elevated-pressure methane/air flames using chemiluminescence emission. Appl Opt 2019;58(10):C61–7.
[4] Hult J, et al. Quantitative three-dimensional imaging of soot volume fraction in turbulent non-premixed flames. Exp Fluids 2002;33(2):265–9.
[5] Ma L, et al. 3D flame topography and curvature measurements at 5 kHz on a premixed turbulent Bunsen flame. Combust Flame 2016;166:66–75.
[6] Wang Q, Zhao C, Zhang Y. Time-resolved 3D investigation of the ignition process of a methane diffusion impinging flame. Exp Therm Fluid Sci 2015;62:78–84.
[7] Floyd J, Kempf A. Computed tomography of chemiluminescence (CTC): high resolution and instantaneous 3-D measurements of a matrix burner. Proc Combust Inst 2011;33(1):751–8.
[8] Li X, Ma L. Capabilities and limitations of 3D flame measurements based on computed tomography of chemiluminescence. Combust Flame 2015;162(3):642–51.
[9] Xu W, et al. 3D flame topography obtained by tomographic chemiluminescence with direct comparison to planar Mie scattering measurements. Appl Opt 2015;54(9):2174–82.
[10] Gragston M, et al. Single-shot nanosecond-resolution multiframe passive imaging by multiplexed structured image capture. Opt Express 2018;26(22):28441–52.
[11] Gragston M, et al. Multiplexed structured image capture to increase the field of view for a single exposure. OSA Contin 2019;2(1):225–35.
[12] Gragston M, Smith CD, Zhang Z. High-speed flame chemiluminescence imaging using time-multiplexed structured detection. Appl Opt 2018;57(11):2923–9.
[13] McCord Walker, et al. Two-phase accurate multiplexed structured image capture (2pAc-MUSIC). Optics and Lasers in Engineering 2021;142 In press. doi:10.1016/j.optlaseng.2021.106621.
[14] Bernini N, et al. Real-time obstacle detection using stereo vision for autonomous ground vehicles: A survey. In: Proceedings of the international IEEE conference on intelligent transportation systems (ITSC), IEEE; 2014.
[15] Ng WB, Zhang Y. Stereoscopic imaging and reconstruction of the 3D geometry of flame surfaces. Exp Fluids 2003;34(4):484–93.
[16] Yu L, Pan B. Single-camera stereo-digital image correlation with a four-mirror adapter: optimized design and validation. Opt Lasers Eng 2016;87:120–8.
[17] Heikkila J, Silven O. A four-step camera calibration procedure with implicit image correction. In: Proceedings of the IEEE computer society conference on computer vision and pattern recognition, IEEE; 1997.
[18] Zhang Z. A flexible new technique for camera calibration. IEEE Trans Pattern Anal Mach Intell 2000;22(11):1330–4.
[19] Bradski G, Kaehler A. Learning OpenCV: computer vision with the OpenCV library. O'Reilly Media, Inc; 2008.
[20] Faugeras O, et al. Real time correlation-based stereo: algorithm, implementations and applications. Inria; 1993.

[21] Fusiello A, Trucco E, Verri A. A compact algorithm for rectification of stereo pairs. Mach Vis Appl 2000;12(1):16–22.
[22] Gordon R. A tutorial on ART (algebraic reconstruction techniques). IEEE Trans Nucl Sci 1974;21(3):78–93.
[23] Huang QX, et al. Reconstruction of soot temperature and volume fraction profiles of an asymmetric flame using stereoscopic tomography. Combust Flame 2009;156(3):565–73.
[24] Jin Y, et al. Three-dimensional dynamic measurements of CH* and C2* concentrations in flame using simultaneous chemiluminescence tomography. Opt Express 2017;25(5):4640–54.
[25] Denisova N, Tretyakov P, Tupikin A. Emission tomography in flame diagnostics. Combust Flame 2013;160(3):577–88.